

Edelstein Effect in Type-II Weyl Semimetal WTe_2 up to Room Temperature

Bing Zhao^{1,2}, Bogdan Karpiak², Dmitrii Khokhriakov², Anamul Md. Hoque², Xiaoguang Xu¹, Yong Jiang¹,
Saroj P. Dash^{2,3,*}

¹Beijing Advanced Innovation Center for Materials Genome Engineering, School of Materials Science and Engineering,
University of Science and Technology Beijing, Beijing 100083, China

²Department of Microtechnology and Nanoscience, Chalmers University of Technology, SE-41296, Göteborg, Sweden

³Graphene Center, Chalmers University of Technology, SE-41296 Göteborg, Sweden.

Abstract

An outstanding feature of topological quantum materials is the current-induced spin polarization due to the unique spin-momentum locking (SML) characteristics of topological states. However, electrical creation and detection of spin polarization of Dirac surface states in topological insulators by reliable non-local methods as well as the spin injection functionality into non-magnetic materials are so far limited to cryogenic temperatures due to the parallel bulk band conduction issues. Here, we report current-induced spin polarization, i.e. the Edelstein effect (EE) and its inverse phenomenon (IEE) in type-II Weyl semimetal WTe_2 up to room temperature. Contrary to the conventional spin Hall and 2D Rashba-Edelstein effects, our measurements show an out-of-plane electrical field-induced spin polarization in WTe_2 due to SML of the spin-polarized bulk Fermi states. Such perpendicular spin-current channel is possible in WTe_2 due to its lower crystal symmetry, large Berry curvature and spin-orbit interaction (SOI) with a novel spin-texture of the bulk bands. We demonstrate the robust electrical creation and detection of spin polarization by EE and IEE, respectively, and utilized such spin polarization to efficiently induce a non-equilibrium spin accumulation in the adjacent graphene channel up to room temperature. These findings open opportunities for utilizing topological Weyl materials as non-magnetic spin sources in all-electrical van der Waals spintronic circuits and understanding their novel spin functionalities at ambient temperature by design of crystal symmetry, SOI, Berry curvature and their spin textures.

Keywords: Weyl-semimetal, Type-II, WTe_2 , spin-momentum locking, Edelstein effect, Graphene, van der Waals heterostructures, current-induced spin polarization, charge-spin conversion, Inverse Edelstein effect.

Corresponding author: **Saroj P. Dash**, Email: saroj.dash@chalmers.se

Department of Microtechnology and Nanoscience, Chalmers University of Technology, SE-41296, Göteborg, Sweden

Main

Topological quantum materials have attracted significant attention in condensed matter physics and spintronic technology because of their unique electronic bands with topologically protected spin textures¹. After the realization of graphene, topological insulators (TIs) and semimetals with Dirac Fermions, Weyl semimetals (WSMs) where the electrons behave as Weyl Fermions have been discovered². The WSMs constitute topologically secured Weyl nodes, which exist with opposite chirality in the bulk with linear band dispersions in three-dimensional momentum space forming the Weyl cones³. The most fascinating revelation in a WSM is the presence of nontrivial Fermi-arc surface states that connect the projections of Weyl nodes on the surface Brillouin zone. In a recent breakthrough, WSMs of type-I and -II are realized in TaAs and WTe₂ family of materials with symmetric and tilted Weyl cones, respectively^{4,5}.

The WTe₂ with low crystal symmetry hosts unique transport phenomena such as chiral anomaly^{6,7}, unconventional quantum oscillations⁸, huge magnetoresistance⁹, spin-orbit torque^{10,11}, large spin Hall effect¹² and quantum spin Hall states in monolayers¹³, which opens a new era for physics experiments. Most importantly, novel spin texture has been discovered in WSMs by photoemission experiments, showing spin polarization of Fermi pockets in bulk bands and Fermi arc surface states^{14,15}. In such WSMs, the application of an electric field is expected to induce a macroscopic spin polarization, known as the Edelstein effect¹⁶, that can be utilized to efficiently generate and detect spin currents. However, it has not been experimentally realized yet. Previously, in the search for spin-polarized sources, various experiments have been reported on TIs¹⁷. However, a reliable non-local measurement for spin polarization in TIs and its utilization for spin injection into non-magnetic materials are so far limited to cryogenic temperatures (below 20K)^{18,19}, because of the interference from non-trivial bulk bands¹⁷. Therefore, finding a highly efficient spin-polarized topological material at room temperature is indispensable for practical applications in spintronics and quantum technologies.

Here, we report a highly efficient current-induced spin polarization, i.e. Edelstein effect (EE) and its inverse phenomena (IEE), in the type-II Weyl semimetal candidate WTe₂ up to room temperature. Importantly, we detect an out-of-plane electrical field-induced spin polarization in WTe₂ due to spin-momentum locking of the polarized bulk Fermi states, which is different from the conventional spin Hall effect²⁰ and 2D Rashba-Edelstein effect (REE)²¹. Finally, the detection of both the EE and IEE prove the robustness of bulk spin polarization in WTe₂ obeying Onsager reciprocity relation and its utilization for spin injection and detection in graphene in an all-electrical van der Waals spintronic device at room temperature.

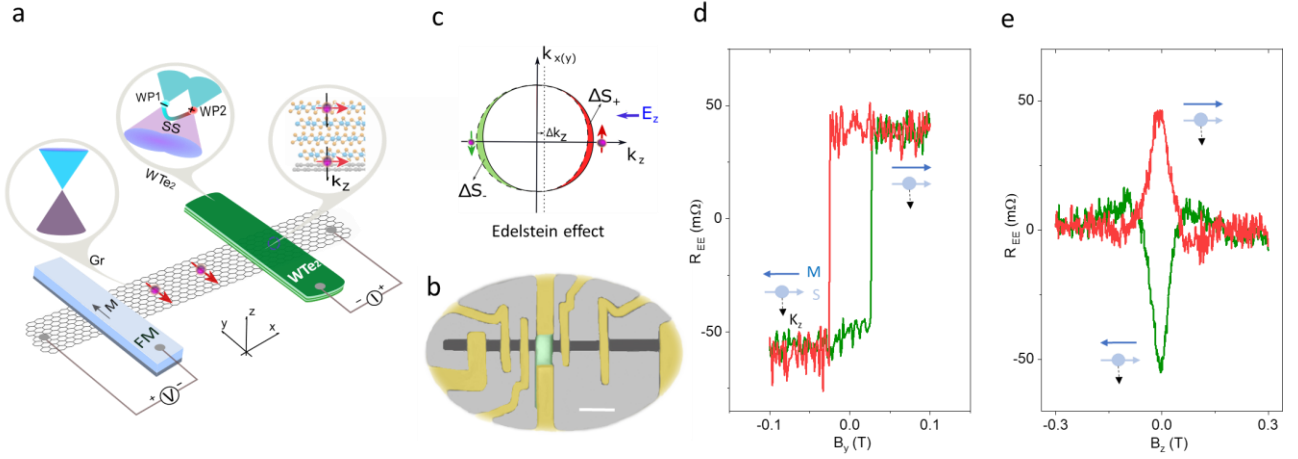


Figure 1. Electrical detection of Edelstein effect in WTe_2 at room temperature. **a,b** Schematic of measurement geometry and device picture (the scale bar is $5 \mu\text{m}$) for electrical detection of Edelstein effect in WTe_2 . The investigated device structure consists of a flake of WTe_2 (green) in van der Waals heterostructure with a graphene channel (gray). The ferromagnetic tunnel contact on graphene is used to detect the current-induced spin polarization of WTe_2 . The insets in the schematics show the simplified type-II Weyl semimetal band structure, spin-momentum locking due to perpendicular current component k_z and the Dirac band of graphene. **c.** Illustration of the Edelstein effect (EE), where a spin accumulation ($\Delta S = \Delta S_+ - \Delta S_-$) is generated by a shift of the Fermi contour (Δk_z) caused by a charge current density E_z along $-k_z$. **d, e.** The nonlocal spin-valve measurement ($R_{EE} = V_{EE}/I$, I is the bias current) and corresponding Hanle spin precession signal observed for parallel and anti-parallel orientation of the injected spin (s) from WTe_2 and magnetization of ferromagnet (M) with positive and negative magnetic field B sweep directions at $I_{dc} = +50 \mu\text{A}$ and 300K in Dev 1.

The measurement of EE and IEE has been possible by employing a hybrid device structure of WTe_2 with graphene channel and ferromagnetic tunnel contacts in a reliable non-local (NL) device geometry. We fabricated van der Waals heterostructures of WTe_2 with graphene taking advantage of its layered structure. The schematics and the nanofabricated device picture are shown in Fig. 1a and 1b respectively, which consists of WTe_2 -graphene heterostructure with ferromagnetic tunnel contacts (see Methods). The graphene (CVD monolayer and exfoliated few layers) and the WTe_2 (20-70 nm in thickness) are exfoliated from single crystals (from Hq Graphene). The Raman spectroscopy characterization shows the T_d -bulk phase of WTe_2 at room temperature (see Supplementary Fig. S1a) and a low temperature $1T'$ structure is known to exist. Crystal structure of WTe_2 has a lower symmetry, with the space group $Pmn2_1$ for bulk WTe_2 crystals with only one mirror plane (bc plane) and without two-fold rotational invariance^{10,22}. The heterostructures of WTe_2 with graphene show good contact properties with interface resistance in the range of 1-3 k Ω (see Supplementary Fig. S1b). The standard spin injection and detection behavior of ferromagnetic tunnel contacts and spin transport properties of graphene were confirmed as shown in the Supplementary Fig. S2.

For the measurement of the Edelstein effect (Fig. 1c), an electric current is applied vertically through the WTe_2 flake, which generates and injects a spin current into the graphene channel (Fig. 1a). The spin polarization is detected by a ferromagnetic Co/TiO₂ contact (FM) after transport in a graphene channel by a NL measurement method. Figure 1d shows the NL spin-valve resistance ($R_{EE}=V_{EE}/I$) for bias current of $I = +50 \mu A$ with an in-plane magnetic field (B_y) sweep at room temperature. The spin resistance R_{EE} changes upon reversing the magnetization M direction of the FM detector with respect to the directions of the injected spins (s) from the WTe_2 . To prove that the origin of the signal is purely due to a spin current, the Hanle measurements were performed with a perpendicular magnetic field B_z sweep along the z -axis (Fig. 1e). Hanle effect induces precession of the spins injected from WTe_2 and transported in the graphene channel about the B_z field with Larmor frequency of $\omega_L=g\mu_B B_z/\hbar$ (where g is the Lande factor=2 and μ_B is Bohr magneton) as the projection of the spin current onto the magnetization of the detector ferromagnet change. In different devices, we extracted spin parameters (with spin diffusion length 0.8–2.4 μm , spin lifetime in the range 100–400ps) by fitting the Hanle signals (see Supplementary Table 1). The spin injection signal from WTe_2 into graphene is reproducibly observed in several devices (six devices were investigated) consisting of both monolayer and few-layer graphene channel with 20–70 nm thick WTe_2 flakes (Supplementary Fig. S3 and S4). The observation of both the spin valve and Hanle signal is the direct and unambiguous evidence of the creation of current-induced spin polarization in WTe_2 and subsequent spin current injection and transport in the graphene channel at room temperature.

In a WTe_2 - graphene hybrid device, the source of the spin polarization can have several origins, such as spin Hall effect (SHE) and Edelstein effect (EE) from the bulk WTe_2 , Rashba-Edelstein effect (REE) from the surface states¹², and proximity-induced SHE and REE in graphene²³. Moreover, some of these effects can induce the in-plane spin polarization and can be entangled with each other. To distinguish different sources of the spin polarization and to identify the origin of the induced spin current in our WTe_2 device, control experiments with geometrical dependence were performed. We first examine the bias current direction dependence of the EE signal (Fig. 2a), where the direction of the generated spins s in the WTe_2 is found to be dependent on the polarity of the applied current bias. Reversing the bias current direction ($I_{dc} = \pm 50 \mu A$) locks the spins in WTe_2 in the opposite direction, resulting in an opposite spin polarization and hence an inverted hysteretic behavior of the measured spin-valve signal (Fig. 2a). These measurements show that the direction of spin polarization can be controlled by electrical means and the spin density is observed to scale linearly with the applied bias current (see Supplementary Fig. S3). The linear bias dependence and a sign reversal behavior with bias current directions rule out the thermal contributions in the measured signal^{24,25}.

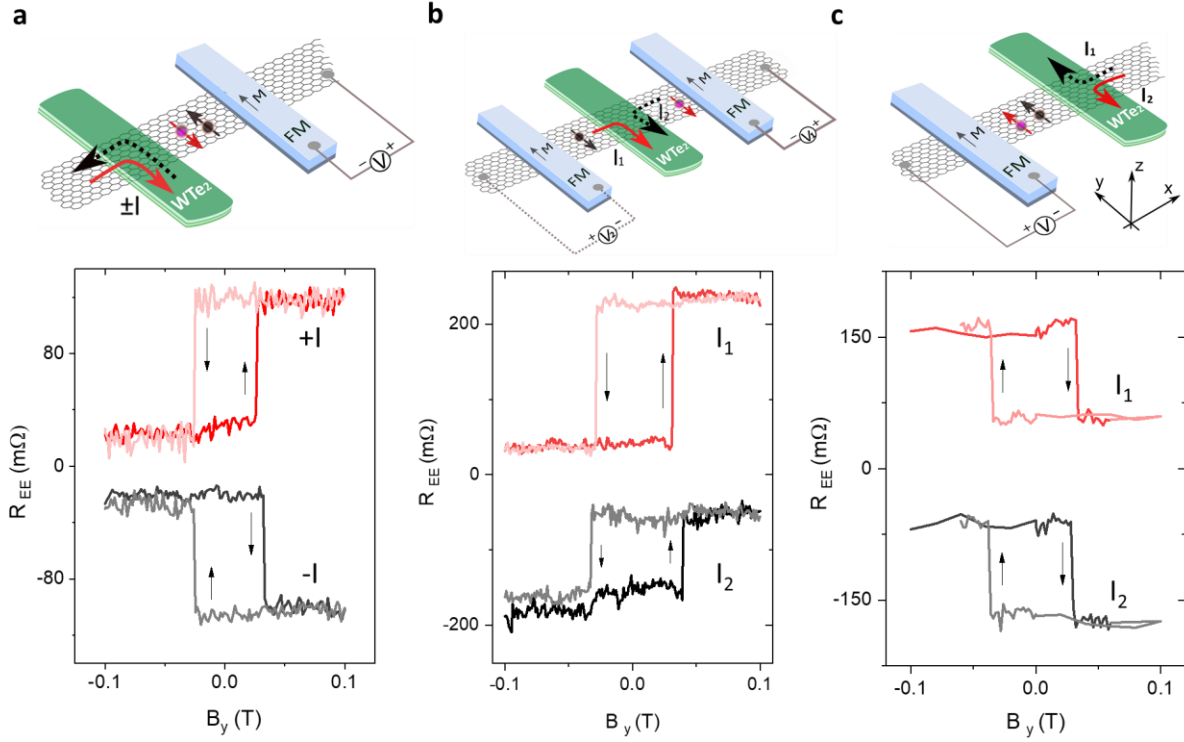


Figure 2. Geometry dependence of the Edelstein effect in WTe₂. **a.** Schematics of the measurement geometry (solid and dash arrows show the applied bias current directions) and the corresponding EE signal with reversal of bias current polarity in Dev 1. The arrows show the switching direction of the signals. **b.** Schematics of the measurement with bias current applied at both sides of the WTe₂ flake and corresponding spin valve signals measured in Dev 2. This measurement creates a reversal of the component K_x of the bias current. **c.** Schematics of the measurement with bias current applied at both terminals of the WTe₂ flake and the corresponding spin valve signals measured in Dev 3. This measurement creates a reversal of the component K_y of the bias current.

The charge current applied in WTe₂ can have three components, i.e. K_x , K_y , and K_z that can possibly induce the spin polarization (see schematics in Supplementary Fig. S5). We performed control experiments by reversing the bias current polarity along different directions to check the polarity of EE signals. As shown in Fig. 2b, the switching directions of EE signal (R_{EE}) remain the same with the reversal of bias currents along both sides of the WTe₂ flake, i.e. the K_x and $-K_x$ directions. Therefore, the bias current component in K_x direction is not the source for the current-induced spin polarization. Consequently, we can rule out the origins of spin polarizations entangled to K_x -direction, like SHE and REE effect in WTe₂¹², and also proximity-induced SHE and REE in graphene^{26–30}. Secondly, when the bias current was applied either to one or the opposite terminal (K_y and $-K_y$ directions) of WTe₂ (Fig. 2c), the R_{EE} signal switching directions remain the same. This rule out the contribution to the spin polarization from the current component in K_y direction. Both the control experiments in K_x and K_y directions were reproduced in other batches of devices (see Supplementary Fig. S6 and Fig. S7). To be noted, the switching direction of devices on different chips are observed to be different (Fig. 2b

and 2c), which can be due to the differences in the orientation of the devices with respect to the magnetic field directions (+/- B) (see details in Supplementary Note 2).

All these control experiments indicate that the current component in K_z direction in WTe_2 is the main source for the generation of spin polarization in the measurement geometry of WTe_2 -graphene devices. Therefore, we attribute the origin of the spin signal to the Edelstein effect in WTe_2 due to the out-of-plane current-induced spin momentum locking of the spin-polarized Fermi states at room temperature^{14,15}. Moreover, the out-of-plane current component along K_z can have two contributions: one through the bulk states $K_{z,B}$; and the other via the surface states $K_{z,S}$ (Supplementary Fig. 5c). From the recent ARPES measurement on WTe_2 ³¹, it is clear that the surface states indeed do not disperse with k_z over an entire Brillouin zone and are thus fully two-dimensional (2D) in the k_x - k_z plane, i.e. straight lines at the edge of the bulk electron and hole pockets. The application of an external electrical field in k_z direction would change the occupation of states and thereby "shift" the Fermi lines. However, due to the small extension of the Fermi line, the area ΔS would be vanishing small, thus, nearly no states would contribute. In other words, since the states do not disperse in k_z direction, their velocity v_z vanishes and no transport is induced by the external electric field in the z-direction. Therefore, we believe, the Edelstein effect observed here in WTe_2 is due to the spin polarized bulk Fermi states.

To further confirm the orientation of spin polarization from WTe_2 , we also performed the angle-dependent measurements of the EE signals both with in-plane and out-of-plane B field sweeps in Dev 4 (see Supplementary Fig. S8). The measured EE signal is observed to evolve from a spin valve signal to a Hanle signal with changing the angle from 0 to 90 deg. Considering the direction of the spin current I_s , the spin polarization s and bias current K_z , the contribution of SHE from WTe_2 can also be ruled out. These systematic measurements again support the observation of the EE in bulk WTe_2 . The EE measurements in WTe_2 using both the spin valve and Hanle geometry were also performed as a function of gate voltage (V_g) in Dev 4 (see Supplementary Fig. S9), where an enhancement of the EE signal magnitude is observed close to the Dirac point of graphene. As the metallic WTe_2 channel resistance does not show any obvious modulation with V_g (Supplementary Fig. S10), the increase of EE signal can be attributed to the increase in graphene channel resistance in the heterostructure and conductivity matching issues at the interface (Supplementary Fig. S9c). However, in the conventional spin valve signals with both FM injector and detector contacts on graphene, a small modulation of spin signal magnitude is observed (Supplementary Fig. S10)³². This increasing trend of EE signal with V_g suggests a possible enhancement of the spin injection efficiency from WTe_2 to graphene near the graphene Dirac point.

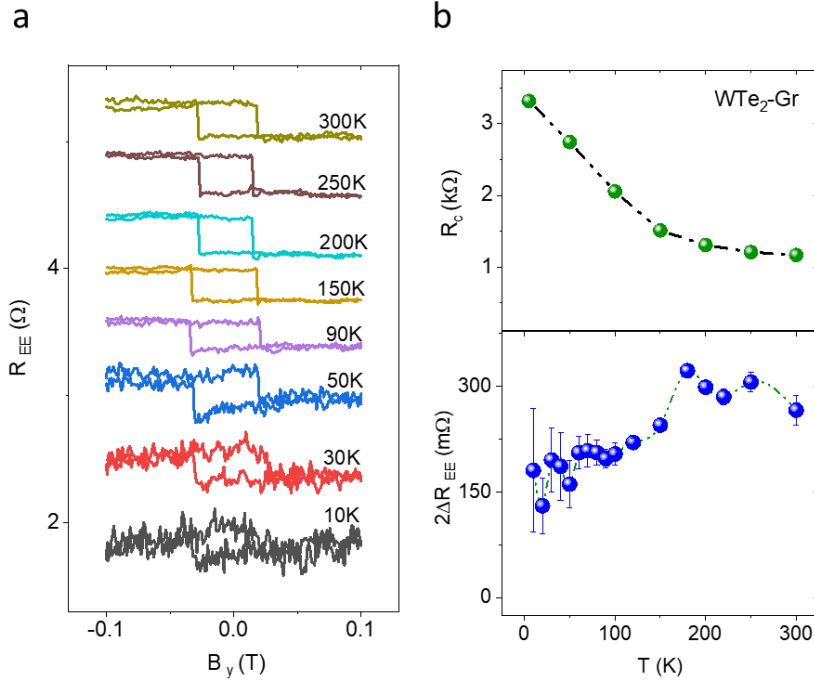


Figure 3. Temperature dependence of Edelman effect in WTe_2 . **a.** Temperature dependence of the Edelman effect in WTe_2 ($R_{EE}=V_{EE}/I$, with $I=-50\mu A$ in Device 2 in the range of 10-300 K. **b.** Top panel: Temperature dependence of the WTe_2 -graphene interface resistance. Bottom panel: Temperature dependence of the EE signal magnitude. The error bars are estimated from the noise in the measured EE signal.

Next, the temperature-dependent measurements of the EE in WTe_2 were carried out to correlate the basic characteristics of the Weyl materials and their spin polarization. The WTe_2 has been experimentally verified to be a type-II Weyl semimetal by observing the negative magnetoresistance^{8,33} and the anomalous-quantum oscillation⁸ at low temperatures. However, the verification of WTe_2 to be a type-II Weyl semimetal at room temperature is still under debate^{31,34,35}, because the momentum difference for Weyl points (WPs) is beyond the resolution of ARPES measurement^{31,36,7}. Hence, it is intriguing to check the temperature dependence of the signal and its relationship with the possible Weyl phase transition at a lower temperature^{8,33}. Figure 3a shows the temperature dependence of the EE signals from WTe_2 , measured in Dev 2 in the temperature range of 10 – 300 K at a fixed bias current $I = -50\mu A$. The switching direction of the measured EE signal in WTe_2 remains the same throughout the temperature range indicating that the origin of the spin polarization remains the same. The obvious slightly larger switching field observed for the signal at lower temperatures is due to an increase in the coercive field of the FM detector contact. The modulation of the magnitude of the EE signal of WTe_2 is plotted with temperature in Fig. 3b (lower panel), where two different regimes were observed. The signal magnitude is weakly temperature-dependent in the range 175 – 300K, whereas a notable decrease is observed below 175K. As spin transport parameters in graphene are known to weakly dependent on temperature³⁷, we identified that the decrease in EE magnitude can be due to the increase in WTe_2 -graphene contact resistance

at lower temperatures (Fig. 3b upper panel). The increase in WTe_2 -graphene contact resistance could cause a decrease in spin injection efficiency from WTe_2 into graphene, while the other parameters were very stable with temperature (see Supplementary Fig. S11). The increased noise level in the EE signal at the lower temperature can also be due to the larger WTe_2 -graphene contact resistances. All these measurements suggest that the observed bulk EE effect is robust from 10K to room temperature and the spin-polarized bulk Fermi states in WTe_2 should be present through all the measured temperature range.

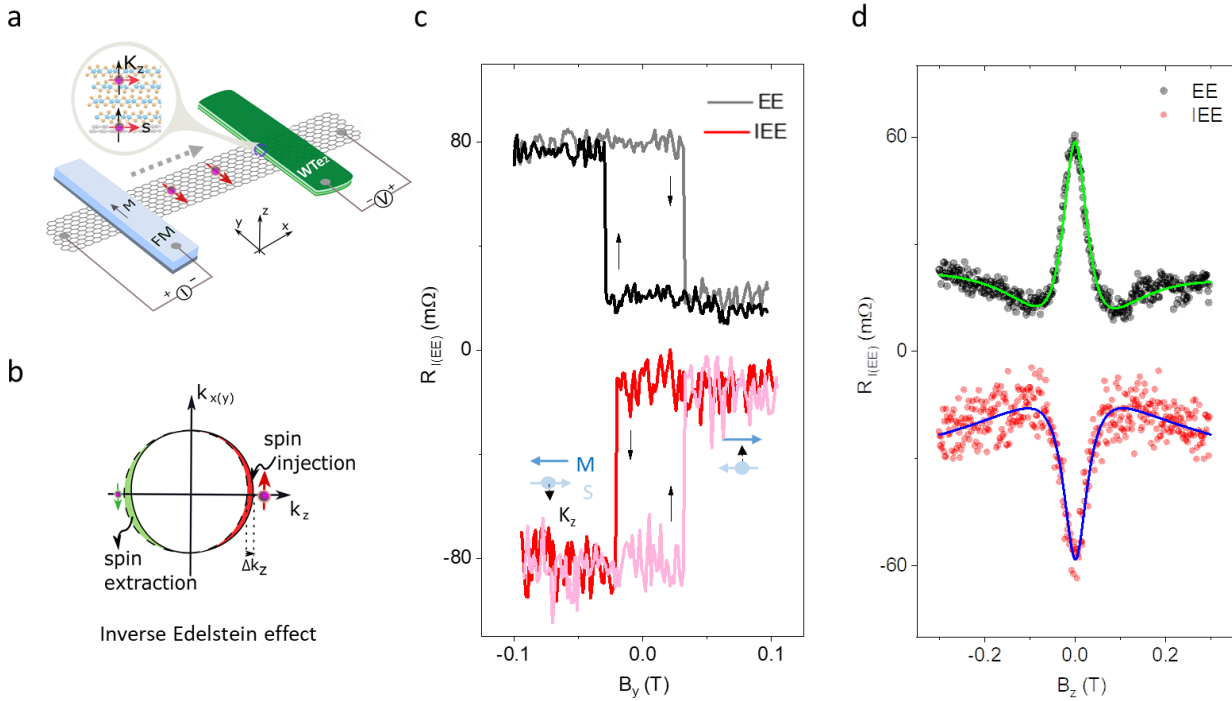


Figure 4: Inverse Edelstein effect in WTe_2 at room temperature. **a.** Schematics of the inverse Edelstein effect (IEE) measurement configuration with spin current injected into the WTe_2 from the FM/graphene structure. **b.** Illustration of the IEE, where a spin polarization along the y -axis is injected into the WTe_2 , leading an extra population (injection) at $+K_z$ of the Fermi contour, while a depletion (extraction) at $-K_z$ part. This results in a net charge current along the z -axis. **c, d.** Measured data of both spin valve and corresponding z Hanle signal with the fitting curve for both EE and IEE in Device 1 with an application of $I = -70 \mu A$ at room temperature. The Hanle signal of the (I)EE is defined by $R_{||EE} = (V_{||EE}(P) - V_{||EE}(AP)) / (2 * I)$.

To check the reciprocity³⁸ of the Edelstein effect in WTe_2 , the inverse Edelstein effect (IEE)^{39,40} measurements were also performed at room temperature (see Fig. 4a). Here, the spin current is injected from an FM tunnel contact into a graphene channel and subsequently detected by the WTe_2 due to the IEE effect in a NL measurement geometry. The spin current with spin polarization s along the y -axis is absorbed into the WTe_2 , leading an extra accumulation spin population (injection) at the $+K_z$ of the Fermi contour, while a depletion (extraction) at $-K_z$ ⁴¹ (Fig. 4b). This results in a net charge current in the K_z direction in the WTe_2 flake. By reversing the FM magnetic moments by an external

in-plane magnetic field sweep, the opposite spins $-s$ are injected into the graphene channel and subsequently absorbed by the WTe_2 , which induces a charge current $-K_z$. A clear hysteric switching behavior of the measured voltage signal is observed with B_y magnetic field sweep, with the switching fields corresponding to the magnetization switching of the spin injector FM electrode (Fig. 4c). Importantly, both the IEE and EE signals measured in the same device show a good Onsager reciprocity with comparable signal magnitude and opposite switching directions, i.e. $R_{EE}(B)=R_{IEE}(-B)$ (Fig. 4c). The IEE effect is reproducibly observed in different devices and the magnitude of the signal is also found to scale linearly with spin injection bias current and changes sign with the bias polarity (see Supplementary Fig. S12 for data on Dev 2). As a confirmatory test for the observed IEE effect, corresponding Hanle spin precession measurements were also performed with application of an out-of-plane magnetic field B_z in the same NL measurement geometry. Figure 4d shows the measured modulation of signal $R_{IEE}=V_{IEE}/I$ as detected by IEE in WTe_2 due to spin diffusion and precession in the graphene channel.

We estimate the bulk EE charge-spin conversion efficiency $\alpha_{(I)EE}$ in WTe_2 to be up to 9% by fitting the Hanle curves of (I)EE signals (see details in Supplementary Note 1). The calculated Edelstein length $\lambda_{EE}=\alpha_{(I)EE}\lambda_{WTe_2}\approx 0.72\text{nm}$ (considering $\lambda_{WTe_2}=8\text{nm}^{12}$). The observed large charge-spin conversion efficiency in WTe_2 is believed to be due to the spin polarization of bulk states, broken space inversion symmetry and a significant influence of SOI in WTe_2 as known from the band structure calculations and spin-resolved ARPES results¹⁵. Interestingly, our measurements show that the charge-spin conversion is not restricted at the 2D surface but originates in the bulk Weyl semimetal WTe_2 . From our control experiments we could rule out the origins of the observed spin polarizations related to SHE and REE in WTe_2 ¹², and also proximity induced SHE and REE in graphene^{26–30}. These observations of perpendicular current-induced Edelstein effect are fundamentally different from the conventional REE, which is an interface phenomenon where the spins and current density are confined in the 2D plane^{40,42} as measured in the heterostructures of metals⁴⁰ and oxides⁴³, topological insulator^{41,44}, TMDCs⁴⁵ and in graphene heterostructures with MoS_2 ²⁶, WS_2 ^{27,30}, TaS_2 ²⁸ and $MoTe_2$ ²⁹. Furthermore, electrically created bulk spin polarization in WTe_2 could be injected and detected in the graphene channel at room temperature, avoiding problems existing in topological insulators^{18,19}.

In summary, we demonstrated the electrical creation, detection, and control of the bulk Edelstein effect and its inverse phenomenon in type-II Weyl semimetal candidate WTe_2 up to room temperature. Contrary to conventional bulk spin Hall effect and surface states dominated Rashba-Edelstein effect, the Edelstein effect is shown here to be created in bulk WTe_2 due to a perpendicular current-induced spin-momentum locking. Furthermore, the spin polarization created in WTe_2 is shown to be utilized for spin injection and detection in a graphene channel in an all-electrical van der Waals heterostructure spintronic device at room temperature, which circumvents the problem existing in topological insulators for spin injection into graphene below 20K. Looking forward, such unique spin-polarized electronic states in Weyl semimetal candidates with novel spin topologies and

low crystal symmetries can be further tuned by tailoring their electronic band structure through enhancing their spin-orbit interaction strength and increasing the separation between the Weyl nodes through Berry curvature design. These findings in Weyl semimetals for efficiently transforming the electric current into a spin polarization at room temperature is highly desirable for energy-efficient read-write processes in spintronic memory and information processing technologies.

Methods

The devices with monolayer CVD graphene on Si/SiO₂ substrate (from Groltex) was patterned by electron beam lithography (EBL) followed by an O₂ plasma etching. The WTe₂ (from Hq Graphene) flakes were exfoliated and dry transferred on to the CVD graphene in the N₂ atmosphere inside a glovebox. The few layers graphene devices were mechanically transferred onto the n-doped Si substrate with 300 nm SiO₂. The WTe₂ flakes were exfoliated and dry transferred on to the few-layer graphene in by a transfer stage in a class 100 cleanroom environment. For the preparation of ferromagnetic tunnel contacts to graphene, a two-step deposition and oxidation process were adopted, 0.4nm Ti was deposited followed by a 30 Torr O₂ oxidation for 10 mins each, followed by 100 nm Co deposition. Measurements were performed by inside a vacuum cryostat and a PPMS measurement system in the temperature range of 10-300K with a magnetic field and a sample rotation stage. The electronic measurements were carried out using current source Keithley 6221, nanometer 2182A and dual-channel source meter Keithley 2612B.

Data availability

The data that support the findings of this study are available from the corresponding authors on reasonable request.

Acknowledgments

Authors thank Annika Johansson, Ingrid Mertig, and Binghai Yan for useful discussions. The authors at Chalmers University of Technology, Sweden acknowledge financial supports from EU Graphene Flagship (No. 604391), EU FlagEra project (from Swedish Research council VR No. 2015-06813), Swedish Research Council VR project grants (No. 2016-03658), Graphene center and the AoA Nano program at Chalmers University of Technology. The authors from University of Science and Technology, Beijing, China, acknowledge financial supports from the National Basic Research Program of China (Grant No. 2015CB921502) and the National Natural Science Foundation of China (Grant Nos. 51731003, 51471029). Bing Zhao would like to thank the financial support from the program of China Scholarships Council (File No. 201706460036) for his 2-year research at Chalmers.

Author information

Contributions

SPD and BZ conceived the idea and designed the experiments. BZ fabricated and measured the devices together with BK, DK, AMH, SPD at Chalmers University of Technology. BZ and SPD analyzed, interpreted the experimental data, compiled the figures and wrote the manuscript. BK, DK, AMH, XX, YJ discussed the results and provided feedback on the manuscript. SPD supervised the research.

Competing interests

The authors declare no competing financial interests.

Corresponding authors:

Saroj P. Dash, Email: saroj.dash@chalmers.se

References

1. Tokura, Y., Kawasaki, M. & Nagaosa, N. Emergent functions of quantum materials. *Nat Phys* **13**, 1056–1068 (2017).
2. Xu, S.-Y. *et al.* Discovery of a Weyl fermion semimetal and topological Fermi arcs. *Science (80-)* **349**, 613–617 (2015).
3. Armitage, N. P., Mele, E. J. & Vishwanath, A. Weyl and Dirac semimetals in three-dimensional solids. *Rev Mod Phys* **90**, 15001 (2018).
4. Zheng, H. & Zahid Hasan, M. Quasiparticle interference on type-I and type-II Weyl semimetal surfaces: a review. *Adv Phys X* **3**, 1466661 (2018).
5. Yan, B. & Felser, C. Topological Materials: Weyl Semimetals. *Annu Rev Condens Matter Phys* **8**, 337–354 (2017).
6. Nielsen, H. B. & Ninomiya, M. The Adler-Bell-Jackiw anomaly and Weyl fermions in a crystal. *Phys Lett B* **130**, 389–396 (1983).
7. Soluyanov, A. A. *et al.* Type-II Weyl semimetals. *Nature* **527**, 495–498 (2015).
8. Li, P. *et al.* Evidence for topological type-II Weyl semimetal WTe₂. *Nat Commun* **8**, 2150 (2017).
9. Ali, M. N. *et al.* Large, non-saturating magnetoresistance in WTe₂. *Nature* **514**, 205–208 (2014).
10. MacNeill, D. *et al.* Control of spin-orbit torques through crystal symmetry in WTe₂/ferromagnet bilayers. *Nat Phys* **13**, 300–305 (2017).
11. Shi, S. *et al.* All-electric magnetization switching and Dzyaloshinskii–Moriya interaction in WTe₂/ferromagnet heterostructures. *Nat Nanotechnol* **14**, 945–949 (2019).
12. Zhao, B. *et al.* Observation of Spin Hall Effect in Semimetal WTe₂. (2018). doi:arXiv:1812.02113v2
13. Tang, S. *et al.* Quantum spin Hall state in monolayer 1T'-WTe₂. *Nat Phys* **13**, 683–687 (2017).
14. Feng, B. *et al.* Spin texture in type-II Weyl semimetal WTe₂. *Phys Rev B* **94**, 195134 (2016).
15. Das, P. K. *et al.* Layer-dependent quantum cooperation of electron and hole states in the anomalous semimetal WTe₂. *Nat Commun* **7**, 10847 (2016).
16. Johansson, A., Henk, J. & Mertig, I. Edelstein effect in Weyl semimetals. *Phys Rev B* **97**, 085417 (2018).
17. Hasan, M. Z. & Kane, C. L. Colloquium : Topological insulators. *Rev Mod Phys* **82**, 3045–3067 (2010).
18. Vaklinova, K., Hoyer, A., Burghard, M. & Kern, K. Current-Induced Spin Polarization in Topological Insulator-Graphene Heterostructures. *Nano Lett* **16**, 2595–2602 (2016).
19. Voerman, J. A., Li, C., Huang, Y. & Brinkman, A. Spin-Momentum Locking in the Gate Tunable Topological Insulator BiSbTeSe₂ in Non-Local Transport Measurements. *Adv Electron Mater* 1900334 (2019). doi:10.1002/aelm.201900334
20. Sinova, J., Valenzuela, S. O., Wunderlich, J., Back, C. H. & Jungwirth, T. Spin Hall effects. *Rev Mod Phys* **87**, 1213–1260 (2015).
21. Han, W., Otani, Y. & Maekawa, S. Quantum materials for spin and charge conversion. *npj Quantum Mater* **3**, 27 (2018).
22. Brown, B. E. The crystal structures of WTe₂ and high-temperature MoTe₂. *Acta Crystallogr* **20**, 268–274 (1966).
23. Ghiasi, T. S., Kaverzin, A. A., Blah, P. J. & van Wees, B. J. Charge-to-Spin Conversion by the Rashba–Edelstein Effect in Two-Dimensional van der Waals Heterostructures up to Room Temperature. *Nano Lett* **19**, 5959–5966 (2019).

24. Slachter, A., Bakker, F. L., Adam, J.-P. & van Wees, B. J. Thermally driven spin injection from a ferromagnet into a non-magnetic metal. *Nat Phys* **6**, 879–882 (2010).
25. Sierra, J. F. *et al.* Thermoelectric spin voltage in graphene. *Nat Nanotechnol* **13**, 107–111 (2018).
26. Safeer, C. K. *et al.* Room-Temperature Spin Hall Effect in Graphene/MoS₂ van der Waals Heterostructures. *Nano Lett* **19**, 1074–1082 (2019).
27. Ghiasi, T. S., Kaverzin, A. A., Blah, P. J. & van Wees, B. J. Charge-to-Spin Conversion by the Rashba–Edelstein Effect in Two-Dimensional van der Waals Heterostructures up to Room Temperature. *Nano Lett* **19**, 5959–5966 (2019).
28. Li, L. *et al.* Electrical Control of the Rashba-Edelstein Effect in a Graphene/2H-TaS₂ Van der Waals Heterostructure at Room Temperature. *arXiv doi:preprint arXiv:1906.10702* (2019).
29. Hoque, A. M., Khokhriakov, D., Karpiak, B. & Dash, S. P. All-electrical creation and control of giant spin-galvanic effect in 1T'-MoTe₂/graphene heterostructures at room temperature. *doi:preprint arXiv:1908.09367v2*(2019).
30. Benítez, L. A. *et al.* Tunable room-temperature spin galvanic and spin Hall effects in van der Waals heterostructures. *doi:arXiv:1908.07868v1*(2019).
31. Bruno, F. Y. *et al.* Observation of Large Topologically Trivial Fermi-Arcs in the Candidate Type-II Weyl Semimetal WTe₂. *Phys Rev B* **94**, 121112 (2016).
32. Han, W. *et al.* Tunneling Spin Injection into Single Layer Graphene. *Phys Rev Lett* **105**, 167202 (2010).
33. Wang, Y. *et al.* Gate-tunable negative longitudinal magnetoresistance in the predicted type-II Weyl semimetal WTe₂. *Nat Commun* **7**, 1–6 (2016).
34. Zhang, W. *et al.* Quasiparticle interference of surface states in the type-II Weyl semimetal WTe₂. *Phys Rev B* **96**, 165125 (2017).
35. Rößmann, P. *et al.* Universal scattering response across the type-II Weyl semimetal phase diagram. *Phys Rev B* **97**, 075106 (2018).
36. Wang, C. *et al.* Observation of Fermi arc and its connection with bulk states in the candidate type-II Weyl semimetal WTe₂. *Phys Rev B* **94**, 241119 (2016).
37. Kamalakar, M. V., Groenveld, C., Dankert, A. & Dash, S. P. Long distance spin communication in chemical vapour deposited graphene. *Nat Commun* **6**, 6766 (2015).
38. Onsager, L. Reciprocal Relations in Irreversible Processes. I. *Phys Rev* **37**, 405–426 (1931).
39. Shen, K., Vignale, G. & Raimondi, R. Microscopic theory of the inverse Edelstein effect. *Phys Rev Lett* **112**, 1–5 (2014).
40. Sánchez, J. C. R. *et al.* Spin-to-charge conversion using Rashba coupling at the interface between non-magnetic materials. *Nat Commun* **4**, 2944 (2013).
41. Rojas-Sánchez, J.-C. *et al.* Spin to Charge Conversion at Room Temperature by Spin Pumping into a New Type of Topological Insulator: α -Sn Films. *Phys Rev Lett* **116**, 096602 (2016).
42. Edelstein, V. M. Spin polarization of conduction electrons induced by electric current in two-dimensional asymmetric electron systems. *Solid State Commun* **73**, 233–235 (1990).
43. Song, Q. *et al.* Observation of inverse Edelstein effect in Rashba-split 2DEG between SrTiO₃ and LaAlO₃ at room temperature. *Sci Adv* **3**, 1–7 (2017).
44. Wang, H. *et al.* Surface-State-Dominated Spin-Charge Current Conversion in Topological-Insulator–Ferromagnetic-Insulator Heterostructures. *Phys Rev Lett* **117**, 076601 (2016).
45. Shao, Q. *et al.* Strong Rashba-Edelstein Effect-Induced Spin–Orbit Torques in Monolayer Transition Metal Dichalcogenide/Ferromagnet Bilayers. *Nano Lett* **16**, 7514–7520 (2016).